

References

1. "Smoking and Health," report of the Advisory Committee to the Surgeon General of the Public Health Service [PHS Publ. No. 1103 (1964), p. 280]; O. J. Balchum, J. S. Felton, J. N. Jamison, R. S. Gaines, D. R. Clarke, T. Owan, *Am. Rev. Respir. Dis.* **86**, 675 (1962); C. M. Fletcher and C. M. Tinkler, *Br. Med. J.* **1**, 1491 (1961).
2. J. A. Merchant *et al.*, *J. Occup. Med.* **15**, 212 (1973).
3. J. A. Merchant, G. M. Halprin, A. R. Hudson, K. H. Kilburn, W. N. McKenzie, D. J. Hurst, P. Bernanzohn, *Arch. Environ. Health* **30**, 222 (1975).
4. K. H. Kilburn, W. S. Lynn, L. L. Tres, W. N. McKenzie, *Lab. Invest.* **28**, 55 (1973).
5. R. V. Lourenco, M. F. Klimek, C. J. Borowski, *J. Clin. Invest.* **50**, 1411 (1971).
6. A. S. Buist and B. B. Ross, *Am. Rev. Respir. Dis.* **108**, 1078 (1973).
7. J. A. Nadel and J. H. Comroe, *J. Appl. Physiol.* **16**, 713 (1961).
8. B. Eichel and H. A. Shahrik, *Science* **166**, 1424 (1969).
9. Fluorocarbon (FC-80) from 3M Company, Minneapolis, Minn.
10. J. H. Luft, *J. Biophys. Biochem. Cytol.* **9**, 409 (1961).
11. R. L. Stedman, *Chem. Rev.* **68**, 153 (1968).
12. R. J. Stephens, G. Freeman, M. J. Evans, *Arch. Environ. Health* **24**, 160 (1972).
13. T. Dalhamn and A. Rosenberg, *Arch. Otolaryngol.* **93**, 496 (1971).

28 February 1975; revised 11 April 1975

High-Resolution Scanning Electron Microscopy of Bacteriophages 3C and T4

Abstract. *An account is presented of the design and operation of a new scanning electron microscope, and its first application to the study of biological samples. Bacteriophages were chosen because much of their ultrastructure is beyond the resolution of the conventional scanning electron microscope. The new instrument permits examination of bulk samples with a resolution that exceeds, by at least a factor of 2.5, the resolution obtained in the best secondary electron scanning electron microscopes using high brightness guns, and exceeds by an order of magnitude the resolution of standard scanning electron microscopes using tungsten filament guns. It also permits examination of biological samples in scanning transmission mode at resolutions similar to conventional transmission electron microscopes.*

Although the conventional transmission electron microscope (TEM) and scanning electron microscope (SEM) have enabled the biologist to examine tissues, cells, and minute subcellular structures with great clarity, it is now possible with a single high-resolution SEM to obtain resolution comparable to that of the TEM while operating in the scanning transmission mode (STEM), and resolution an order of magnitude better than that of the standard tungsten filament SEM when examining the surface of bulk samples. The surface resolution is also close to that obtained when the TEM is used to examine biological samples. This report presents surface and transmission micrographs obtained in this instrument, a machine which has its origin in several distinctive modifications in electron microscope design, but which has never previously been used for gathering information from bulk samples of biological materials.

Earlier work with this instrument (1) demonstrated that with a lanthanum hexaboride (LaB₆) cathode electron gun and a final lens of short focal length it was possible to produce a beam diameter of 5 Å. Beam diameters of this size had already been obtained with field emission cathodes (2); however, field emission cathodes require a vacuum level of better than 1×10^{-9} torr, which is obtained only at the expense of increased complexity, cost, and inconvenience of use. The LaB₆ cathode can be operated in any well-maintained conventional vacuum system ($< 10^{-5}$ torr)

using elastomer O-rings, and oil diffusion pumps, as on the majority of commercial electron microscopes.

Initial evaluation of this microscope was by STEM. Subsequently, using a concept proposed by Wells (3), a new method for examining bulk samples was found. At that time it had been thought that to form a high-resolution surface image of a bulk sample, it was necessary to collect low-energy secondary electrons from the point of impact of the beam. In order to do this efficiently the sample was always placed outside the magnetic field of the final lens. This necessitated the use of a relatively long focal length final lens with higher aberrations ($C_s = 1.8$ cm, $C_c = 1$ cm) than are encountered in the type of short focal length lens ($C_s = 0.06$ cm, $C_c = 0.07$ cm) (4) used in this microscope. By the new method a bulk sample is placed in the high field region of the lens, and the image formed by collecting primary beam electrons which have been scattered from the sample surface. Wells (5) has called this type of image the low-loss image because most of the electrons collected have lost little energy in the sample (< 1000 eV).

Low-loss SEM images obtained in this way provide detailed surface information at a resolution formerly reserved for TEM. At the same time, the images can be easily interpreted in three dimensions as in the conventional long focal length SEM images. Specimen size and low magnification operation are restricted compared to the standard SEM, because the sample is

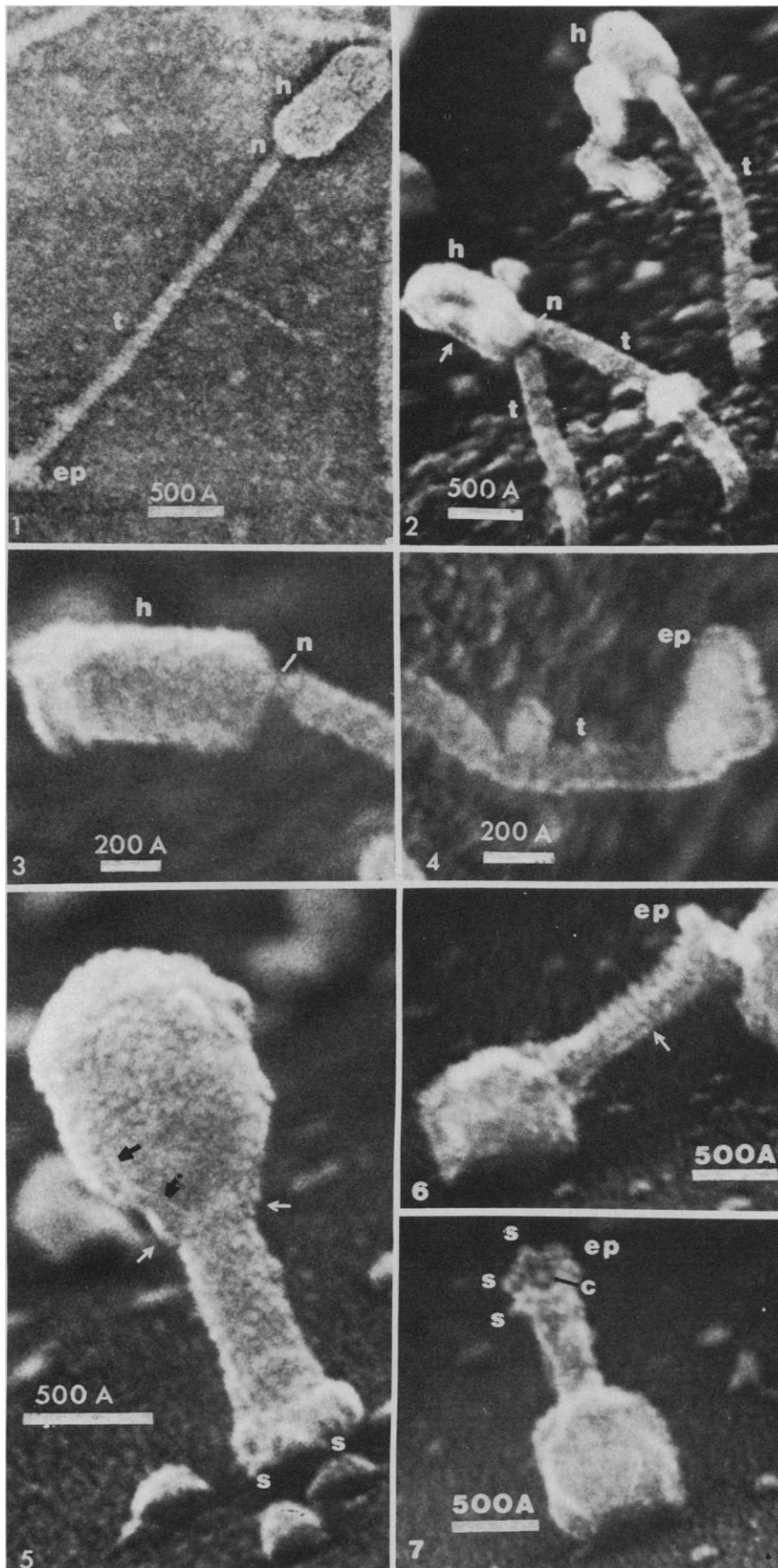
placed in the small lens gap, but this has not proved a significant problem for the examination of small biological samples. In this work we have been able to use the surface mode to observe the morphology of bacteriophages directly, without many of the interpretational problems inherent in transmission electron microscopy. In each case the bacteriophages were also examined in the STEM mode in order to compare our data with previously reported literature in this field.

High-quality secondary images formed with the use of a short focal length final lens SEM have also recently been reported by Kondo and Hasegawa (6). Their results, while showing improvement over standard secondary electron images, do not possess the clarity at high magnification that ours possess. It is unclear whether this is due to the improved electron optical performance obtained with the LaB₆ cathode, or is due to the use of high-energy scattered electrons rather than secondaries.

The final lens of the microscope is of the symmetrical condenser-objective type with bores 3 mm in diameter, and a 3-mm gap. For low-loss SEM, the samples are placed in the center of the pole-piece gap. In this position the lens focal length is 1 mm, the spherical aberration coefficient is 0.06 cm, and the chromatic aberration coefficient is 0.07 cm. A beam half angle of 1.4×10^{-2} radian is employed, giving an estimated beam diameter (containing 80 percent of the beam current) of 10 Å for a current of 2×10^{-11} ampere. The gun brightness has been measured to be 9×10^6 amp/cm² steradian at the accelerating potential (45 keV) used for this work. The beam diameter as estimated from edge definition in the SEM micrographs is close to, or below, the calculated 10 Å. The electron detector for the low-loss surface mode is a quartz light pipe, 1 cm in diameter, coated with scintillator and a thin layer of aluminum. It is placed approximately 14 cm below the lens gap. A diagram of the detector configuration has already been published (3). With the samples examined here, the current reaching the detector varied between 5×10^{-13} amp and 1.5×10^{-12} amp for an incident current to the sample of 2×10^{-11} amp.

For operating in the bright-field STEM mode, an aperture was placed above the scintillator detector. The aperture subtended a half angle of 5×10^{-3} radian at the sample. The beam current for STEM was about 2×10^{-12} amp and the beam diameter was 5 Å.

Log phase *Staphylococcus aureus* (strain 3C), grown on nutrient agar, was inoculated with 3C phage and incubated at 30°C. Samples were taken at 1-, 2-, and 5-hour intervals after inoculation and were



end plate are similar in location and size to the spikes, which function in phage absorption. Rodlike structures (black arrows) are frequently observed extending from the end plate, or lying against the phage tail and projecting up onto the phage head. These may be tail fibers which are partially obscured by the metal coating. Fig. 6. T4 coliphage coated with approximately 25 Å carbon-gold-palladium seems to show a periodicity of the tail sheath (arrow) similar to that described in the literature (11-13). Fig. 7. Clear view of T4 phage end plate (ep) reveals the central core (c) and the sixfold symmetry of the end plate.

prepared for STEM and SEM. A small area of the inoculated plate was scraped with a transfer loop, and the specimens were placed on a Formvar-carbon-coated copper grid. Residual fluid was drained off the grid, and the specimen was stained with 2 percent aqueous, filtered uranyl acetate. Specimens for SEM were taken at the same time and were placed on a silicon dioxide sliver (9 × 1 × 0.4 mm) and fixed in 1.5 percent glutaraldehyde in 0.1M cacodylate buffer (pH 7.4) for 1 to 5 hours at room temperature. The slivers were then washed in 0.1M cacodylate buffer, post-fixed in 1 percent aqueous osmium tetroxide at room temperature, and washed in distilled water. To increase the backscatter yield, some samples were bathed in 2 percent aqueous uranyl acetate for 1 hour (7). Residual stain was removed by washing with distilled water. The specimens were then dehydrated in acetone, dried by the critical point method (8), and coated with a thin layer of carbon-platinum-palladium or carbon-gold-palladium (approximately 50 Å for Figs. 2 to 5, and 25 Å for Figs. 6 and 7).

T4 coliphages were also studied. Log phase *Escherichia coli* (strain B) grown on nutrient agar (to which tryptophan had been added) were inoculated with T4 bacteriophage and grown at 37°C. Samples were taken at 10 and 30 minutes after inoculation and prepared as previously described.

Both staphylococcal phage 3C and T4 coliphage are readily visualized with low-loss SEM and STEM. Micrographs of phage taken on this microscope by STEM (Fig. 1) compare closely with information observable from micrographs of the same specimens taken by high-resolution TEM (9).

Fig. 1. This STEM image of a 3C staphylococcal phage clearly shows the head (h), narrow neck (n), helical tail (t), and knoblike end plate (ep). Stained with 2 percent uranyl acetate. Fig. 2. This low-loss SEM image reveals 3C phage morphology similar to that observed by STEM. A typical cylindrical head (h), and a collapsed head (arrow), characteristic of phages which have lost their nucleic acid, are seen. Fig. 3. At high magnifications, the narrow neck region (n) joining the cylindrical head (h) to the tubular tail (t) is clearly apparent. There seems to be a repeating periodic structure to the tail (diagonally from left to right). Fig. 4. The end plate (ep) possesses tubular projections, similar to those described for type III noncontractile phages. This micrograph also suggests a period to the tail (t). Fig. 5. This untriggered T4 coliphage imaged by low-loss SEM shows the head, collar (white arrows), tail, and end plate. Small projections (s) arising from the

By low-loss SEM, the head (*h*) of the 3C phage appears cylindrical (Figs. 2 and 3). Two slightly different head configurations are observed in SEM, STEM, and TEM micrographs. Most of the phage heads have straight, parallel sides along the vertical (long) axis. Other heads appear swollen; the length of the head remains constant, but the sides of the long axis appear to bulge, or seem dented or collapsed (Fig. 2, arrow). By STEM we find that these bulging or collapsed heads are more transparent, suggesting that they are devoid of nucleic acid. The altered head morphology may be due to capsid fragility after nucleic acid expulsion. When compared to the size of phage heads seen by STEM, those observed by SEM appear uniformly larger. We attribute this fact to the metal coating on the surface of the SEM sample (approximately 50 Å in thickness).

At the point of attachment of the head, the tail (*t*) narrows markedly (*n*), appearing one-half as thick (Figs. 1 to 3). This is similar to the TEM micrographs of Tikhonenko (9), who reported a narrowing of the tail in the neck region (*n*) of negatively stained phage Polonus X of *Mycobacterium tuberculosis*, a similar noncontractile phage. When examined at high magnifications, the end plate of the tail is found to consist of a number of lobular projections (Fig. 4), which corresponds to the postulated type III end plate found in group IV phages (10). To our knowledge this is the first time this structure has been verified.

Low-loss SEM images of the T4 coliphage clearly show the head, tail, and end plate (11) (Figs. 5 to 7). At the junction between the head and tail, there appears to be a band girdling the neck, corresponding to the "tail collar" first reported by Anderson (12) (Figs. 5 and 6, white arrows). In some instances, it seems possible in the SEM image to resolve the period of the helical tail sheath (Fig. 6, white arrow). At the base of the tail there is an enlarged region, and at high magnifications small projections (*s*) can be seen extending from the end plate (Figs. 5 to 7). In cases where the tail is uppermost, the sixfold symmetry of the end plate is clearly seen together with the central core (Fig. 7, black line). STEM images of coliphages show similar spikes projecting from the lower surface of the end plate (13). Also in the untriggered phage, long, thin, threadlike structures extend from the end plate up along the vertical axis of the tail and often project onto the head (Fig. 5, black arrows). These may be the tail fibers that were not obscured by the metal coating. We also find the tail fibers in this position in STEM micrographs.

Small globular particulates are observed on the surfaces of both bacteria and phages (particulate size, 10 to 30 Å) at very high

magnifications (Figs. 5 to 7). These particulates are presumed to be a product of the coating rather than significant biological ultrastructure, because they are also seen on the otherwise smooth surface of the SiO₂ substrate. We have found that the amount of ultrastructural detail that is obscured by the coating is significantly less when the coating thickness is reduced. For example, see Fig. 6 where there is clear evidence of the period of the helical sheath (arrow), whereas in Fig. 5 this periodicity is obscured. The coating in Fig. 6 was 25 Å compared to 50 Å in Fig. 5. It should be possible by refinement of the evaporation technique to further reduce the granularity of the evaporated coating. It may also be that sufficient density can be provided to the specimen by surface doping with material of high atomic number through the use of a binding agent (14). Preliminary experiments in which heavy metal staining procedures have been used to enhance contrast have proven successful (15).

We have successfully shown that surface and internal ultrastructure of phages can be studied at useful magnifications as high as 500,000× and point-to-point resolution approaching 20 Å (7-Å resolution using the "width of the dark space" criterion) by SEM using the low-loss method (2), and by STEM operation of the same instrument at resolution similar to TEM. The clarity of the micrographs, superior resolution, lack of sample charging effects, and versatility of examination of SEM and STEM make this a superior tool for biological ultrastructural research. The technology used in the microscope is quite similar to that used in today's commercial electron microscopes. The limiting factor in high-resolution SEM is not only the instrument,

but equally the specimen preparation, and as with most advances in microscopy, improved methods of specimen preparation are just as important as improvements to the microscope itself.

A. N. BROERS

IBM Thomas J. Watson Research
Center, Yorktown Heights,
New York 10598

B. J. PANESSA

J. F. GENNARO, JR.

St. Vincent's Hospital and
Laboratory of Cellular Biology,
New York University, New York 10003

References and Notes

1. A. N. Broers, *Appl. Phys. Lett.* **22**, 610 (1973).
2. A. V. Crewe and J. Wall, *J. Mol. Biol.* **48**, 375 (1970).
3. O. C. Wells, A. N. Broers, C. G. Bremer, *Appl. Phys. Lett.* **23**, 353 (1973).
4. Lens aberration data obtained from data of M. B. Heritage, IBM Thomas J. Watson Research Center, Yorktown Heights, New York.
5. O. C. Wells, *Appl. Phys. Lett.* **19**, 232 (1971).
6. I. Kondo and N. Hasegawa, *JEOL (Jpn. Electron. Opt. Lab.) News* **12**, 16 (1974).
7. B. J. Panessa and J. F. Gennaro, Jr., in *IITRI Scanning Electron Microscopy/72*, O. Johari, Ed. (IITRI, Chicago, 1972), p. 327.
8. T. F. Anderson, *Trans. N.Y. Acad. Sci.* **13**, 130 (1951).
9. D. Bradley, *J. Ultrastruct. Res.* **8**, 552 (1963).
10. A. Tikhonenko, *Ultrastructure of Bacterial Viruses* (Plenum, New York, 1970).
11. M. Moody, *Virology* **26**, S67 (1965).
12. T. F. Anderson, in *Proceedings of the European Regional Conference on Electron Microscopy, Delft, 1960* (Nederlandse Vereniging voor Electronen Microscopie, Delft, 1960), vol. 2, p. 1008.
13. W. Wood and R. Edgar, in *Molecular Basis of Life*, R. Haynes and P. Hanawalt, Eds. (Freeman, San Francisco, 1968), p. 153.
14. R. O. Kelley, R. A. F. Dekker, J. G. Bluemmik, *J. Ultrastruct. Res.* **45**, 254 (1973).
15. A. N. Broers, B. J. Panessa, J. F. Gennaro, Jr., in *IITRI Scanning Electron Microscopy/75*, O. Johari, Ed. (IITRI, Chicago, 1975), p. 233.
16. We thank the Phage Typing Laboratory and Dr. Oishi of the New York Department of Public Health, and Bill Rosenzweig and Milton Schiffenbauer of New York University, Washington Square, for their assistance in growing the phages. John Sokolowski is also recognized for designing and building many of the critical components of the new SEM.

11 March 1975; revised 15 April 1975

Distribution of Concanavalin A Receptor Sites on Specific Populations of Embryonic Cells

Abstract. *The early 32- to 64-cell stage of the sea urchin embryo consists of three cell types, easily distinguishable by size: micromeres, mesomeres, and macromeres. Only the micromeres are migratory. Treatment of dissociated sea urchin embryo cells with fluorescein-labeled concanavalin A (Con A) revealed a Con A-induced highly clustered or capped distribution of receptor sites on the micromeres. Concanavalin A did not induce significant clustering or capping of receptor sites on the mesomeres or macromeres. The results indicate that Con A receptor sites are more mobile on specific populations of malignant-like migratory embryonic cells.*

Plant lectins, which bind to specific cell surface carbohydrate residues, have been used in recent years to explore many aspects of the structure and function of cell surfaces. One such lectin, concanavalin A (Con A) causes agglutination of transformed cells and embryonic cells, but not their normal or adult counterparts without

previous trypsinization (1). Concanavalin A is capable of binding to nonagglutinable cell types. However, it seems to induce a clustering of Con A binding sites only in the membranes of cell types that are agglutinable (2, 3).

It has been proposed that during morphogenesis the orderly shifts of individual